Glycol Lignin/MAH-g-PP Blends and Composites with Exceptional Mechanical Properties for Automotive Applications

Jonathon Tanks[a*], Kenji Tamura[b], Kimiyoshi Naito[a,c], Thi Thi Nge[d], Tatsuhiko Yamada[d]

[a] *Research Center for Structural Materials, National Institute for Materials Science, 1-2-1 Sengen, Tsukuba, Japan 305-0047*

[b] *Research Center for Functional Materials, National Institute for Materials Science, Tsukuba, Japan 305-0044*

[c] *Department of Aerospace Engineering, Tohoku University, Sendai, Japan 980-8579*

[d] *Center for Advanced Materials, Forestry and Forest Products Research Institute, Tsukuba, Japan 305-8687*

[*]*Email: tanks.jonathon@nims.go.jp; tel.: (+81) 029-859-2606*

Abstract

Lightweight plastics and their composites are being increasingly used in automobiles to reduce emissions and costs, but the market demand for fossil fuel-based plastics such as polypropylene (PP) creates several environmental problems such as pollution and waste. Although replacing PP with biomass such as lignin is not a new endeavor, the vast majority of past studies reported reduced mechanical properties as lignin content increases, which limits its application in industry. Herein, blends of maleic anhydride-grafted PP (MAH-*g*-PP) and softwood-derived glycol lignin (GL) are successfully fabricated via a melt-mixing approach, which boast exceptional mechanical properties and thermal stability. Synergistic performance enhancement is observed when combined with carbon fiber reinforcement, which is elucidated by nanoindentation of the fiber/polymer interface. This work contributes to the development of sustainable automotive structures by efficiently combining biomass and traditional materials.

1. Introduction

Polypropylene is one of the most commonly used commodity polymers in the world, ranging from fabrics, packaging, automotive components, toys, and numerous other applications [1]. Its low density (~0.9 g/cm^3), moderate strength (~30 MPa), high elongation (~900%), and good processability have led to its widespread utilization in automobiles, which contain as much as 20% plastic in an effort to reduce weight and increase fuel efficiency [2]. According to data available in 2014, the typical passenger car contains between 7-8% polypropylene (PP) by weight, translating to roughly 100-120 kg per vehicle [2]. Investigation into fillers and fibers for polypropylene composites has led to increased usage in place of metals, reporting strengths around 60 MPa for 20 wt% carbon fiber with neat PP, but as high as 80 MPa when maleic anhydride-grafted PP (MAH-*g*-PP) is incorporated [3-5]. Low-cost fillers such as talc and nanoclay have also been employed to improve thermal and mechanical properties [2,6-8].

While the replacement of metal with lightweight plastic has improved fuel efficiency in automobiles, PP is a petroleum-based plastic that contributes to greenhouse gas emissions and also accounts for a large amount of plastic waste in oceans and forests, creating a burden on the environment through market supply alone [9]. Various bio-derived and biodegradable plastics have been developed, such as polylactic acid (PLA) and poly(butylene adipate-co-terephthalate) (PBAT) [10-16], but the issues of density (typically 1.2-1.3 g/cm^3) and poor resistance to moisture and UV have hindered their usage in automobiles. Thus, a strategy is required for keeping PP as the base material but using less while achieving target properties in order to limit environmental impact—i.e., blend PP with an environmentally-friendly alternative material.

Lignin constitutes roughly 15-30% of all biomass, and is regarded as the second most abundant biopolymer after cellulose [17]. In addition to serving as a bio-source for thermoplastic and thermoset polymers [10], various approaches have been taken to utilize lignin in polymers with the aim of reducing plastic use, reducing biomass waste, and improving polymer performance. Chemical modifications have been implemented to improve compatibility with the polymer matrix, ranging from acetylation [18-20], alkylation [15,19,21,22], aminosilane coupling [23], alkene-grafting [24], esterification [13,14,16], and etherification and epoxidation [25]. The thermal- and UV-stability of thermoplastics was enhanced by the addition of lignin, primarily due to lignin's ability to scavenge oxidative radicals [19,20,28-30].

However, simultaneous improvement of mechanical properties remains elusive. The combination of unmodified polymer and unmodified lignin expectedly produce the worst performance, with strength reduced to 30-50% for lignin contents ranging from 10 to 40 wt% in thermoplastics such as PP [26], PBAT [12,15], and PLA [16]. Since lignin is rich in functional groups such as hydroxyls, its compatibility with hydrocarbon-based polyolefins (e.g., PP) is poor and must be improved by either alkylation of the lignin, or modification by MAH-*g*-PP. Reductions in strength and stiffness were still reported despite using alkylated lignin, which was attributed to the lignin acting more like a plasticizer than reinforcement [19,21,22]. In the case of MAH-g-PP, ester bonds are formed with hydroxyl groups on the unmodified lignin, and hydrogen bonding also increases so that the reduction in mechanical performance is mitigated even at high loadings [15,24,26,31-34]. A ball-milling approach to controlling the particle size of unmodified lignin showed no significant decrease in mechanical performance at 10 wt% in neat PP [34], but this technique has yet to be demonstrated

for higher loadings. It is crucial that PP/lignin blends for automotive applications retain mechanical properties at least comparable to the neat PP, or else the trade-off between sustainability and performance becomes uneconomical. Significant improvement in both mechanical and thermal properties of polypropylene/lignin blends at high loadings (i.e., >10 wt%) has not been reported (to the authors' knowledge).

Recently, the industrially applicable processing system of polyethylene glycol (PEG)-modified glycol lignin (GL) production from softwood biomass via acid-catalyzed PEG solvolysis was developed [35-38]. As there may be a physical limitation to how well the MAH groups can access the phenol groups on the lignin, the long PEG chains may assist in the bonding processes and lead to greater compatibility. The purpose of this study was to fabricate low-density, low-cost polypropylene/lignin blends and their short carbon fiber composites with enhanced mechanical properties using GL and MAH-*g*-PP, in order to reduce the use of petroleum-based plastics in automobiles while achieving high strength-to-weight performance. Employing twin-screw extrusion, the simple raw materials were mixed in ratios up to 30 wt% GL and 30 wt% carbon fiber; characterization techniques included IR spectroscopy, tensile testing and nanoindentation. The exceptional mechanical properties achieved were compared with similar materials in the literature, and implications for industrial use were discussed.

2. Experimental Methods

2.1.Materials

A commercial MAH-*g*-PP known as ADMER™ QE800E, denoted in this paper as mPP (0.04 wt% MAH [39]), was received from Mitsui Chemicals. The GL used in this study was obtained from PEG400 solvolysis of softwood biomass, where about 26 wt% PEG400 was grafted onto isolated lignin macromolecules (denoted as GL400M in

previous reports [36]). Chopped carbon fibers (PYROFIL™ TR06NLB5K, length × diameter = 6 mm × 7 μm) were purchased from Mitsubishi Chemical.

2.2.Compounding of mPP/GL Blends and Composites

Compound samples were prepared by melt mixing at 240-250 °C using a twin-screw extruder (S1KRC, Kurimoto) equipped with pelletizing system (Figure 1a). The extruded pellets were dried under vacuum at 80 °C overnight to remove moisture. Using an injection molding machine (Mini JET II, Thermo Scientific), the extruded composite pellets were injection molded into ISO standard dumbbell specimens (ISO 527-2) at a cylinder temperature of 250°C and a mold temperature of 40 °C. After molding, the specimens were stored at 23°C for 24 h prior to tensile testing. GL contents of 0, 10, 20, and 30 wt% were combined with CF contents of 0, 10, 20, and 30 wt%, labeled mPP-GL*X*, mPP-CF*X*, or mPP-GL*X*-CF*X*, where *X* indicates the content (wt%).

2.3.Characterization

The specific gravities of the samples were estimated using a densimeter (SD200L, Ektron Tek) according to ASTM D792. Fourier transform infrared (FTIR) spectra were recorded over the range 500–4000 cm^{-1} on a Nicolet 6700 (Thermo Scientific) in transmission mode by cutting 20 μm-thick films from the prepared dumbbell specimens, while ATR mode was used on GL powder and the isolated carbon fiber sizing agent.

Differential scanning calorimetry (DSC) was performed on roughly 3-4 mg of sample under N_2 flow over the range -50-200 °C on a DSC7020 (Hitachi Hi Tech) at rates of 5 and 10 °C/min for heating and cooling, respectively, and the degree of crystallinity χ_c was calculated by the enthalpy of fusion ΔH_m from the melting peaks:

$$\chi_c = \frac{\Delta H_m}{(1-\alpha)\Delta H_m^0} \times 100 \quad (1)$$

where ΔH_m^0 is the enthalpy of fusion of perfectly crystalline polypropylene (taken as 207 J/g) [22], and α is the mass fraction of GL. Thermogravimetric analysis (TGA) was performed on a TG/DTA7300 (Hitachi Hi Tech) by heating approximately 4-5 mg of sample from 20 to 1000 °C under N_2 atmosphere at a rate of 10 °C/min.

Dynamic mechanical analysis (DMA) was performed on a DMS7100 (Hitachi Hi Tech) over temperature and frequency ranges of -100-125 °C and 0.05-100 Hz, respectively; the center portion of dumbbell specimens were deformed with an amplitude of 10 μm in double-cantilever mode under N_2 atmosphere. Activation energies for transitions (denoted as E_x, where x is α, α', or β) were calculated by the Arrhenius equation [40]:

$$f = f_\infty \exp\left(-\frac{E_x}{RT}\right) \quad (2)$$

where f is the loading frequency (proportional to strain rate), f_∞ is the pre-exponential factor, R is the ideal gas constant, and T is temperature. Time-temperature superposition was performed on frequency sweep data over a temperature range of -50-100 °C and the activation energies for rate- and temperature-dependent deformation were calculated by the following Arrhenius relation [40]:

$$\log(a_T) = -\frac{E_a}{R}\left(\frac{1}{T} - \frac{1}{T_0}\right) \quad (3)$$

where a_T is the frequency shift factor and T_0 is a reference temperature (set at 50 °C).

Tensile properties of the fabricated dumbbell specimens were evaluated using an electromechanical testing machine (EZ-LX, Shimadzu) at a crosshead speed of 5 mm/min (as per ASTM D638), and the strain was measured by video extensometer. Nanoindentation was performed using a Hysitron TriboIndenter (Bruker) on mPP-GL20

and mPP-GL20-CF20 dumbbell specimen cross sections that had been polished (down to 0.05 μm alumina slurry). The nanoindentor was equipped with a diamond Berkovich tip (included angle = 142.3°, Young's modulus = 1140 GPa) and a nanoDMA transducer capable of modulus mapping, and scans were taken with a tapping frequency of 200 Hz and amplitude of 0.5-1.0 nm (translating to roughly 4-6 μN). Quasi-static indentation measurements of the fiber and matrix regions were calibrated against fused quartz and PMMA standards, respectively, to produce the reduced modulus values. Fracture surfaces of the dumbbell specimens were analyzed by scanning electron microscopy (Quanta 600 SEM, FEI).

3. Results and Discussion

3.1. Structure and Properties of mPP/GL Blends

3.1.1. Chemical and Thermal Analyses

The expected structure of the mPP/GL blends is shown in Figure 1b, where the PEG and MAH groups form ester bonds and create a sort of flexible crosslink. The chemical composition of each material was confirmed by FTIR (Figure 1c), where the characteristic peaks of mPP and GL are clearly visible in their respective intensities depending on the GL content. The characteristic peaks of PP are located around 2840-2930, 722, 970-1000, 1165, 1375 and 1455 cm^{-1} [26,28]. Additionally, the MAH peaks can be seen at 1732 and 1775 cm^{-1}, which are converted to ester (1733 cm^{-1}) and carboxylic acid (1710 and 3440 cm^{-1}) upon reacting with GL (Figure S1, Supporting Information). GL exhibits several characteristic peaks around 1512, 1592, 1711, and 1086 cm^{-1}, corresponding to aromatic groups, carbonyls, and aliphatic ethers, respectively [35,37]. As the GL content increases, the corresponding GL skeletal peaks increase, as do the –OH peaks resulting from glycol/MAH coupling reactions. In the

case of carbon fiber composites (mPP-GL-CF), the GL may also form bonds with the polyester-based fiber sizing (Figure S1, Supporting Information). Detailed discussion on DSC and TGA results can be found in the Supporting Information. In brief, the results show that mPP-GL blends exhibit similar melting behavior as neat mPP and improved thermal stability, which is advantageous for processing and in-use performance.

3.1.2. Physical and Tensile Properties

The densities of the mPP/GL compositions were between 0.9-1.1 g/cm^3, even when replacing 50wt% of mPP with GL and CF. The tensile properties of all blends and composites in this study are summarized in Table 1. The percentage increase compared to neat mPP is given in parentheses. Since energy efficiency is crucial for automotive structures both in terms of financial and environmental costs, density near ~1.0 g/cm^3 is advantageous [2]. The tensile properties of the mPP-GL blends are summarized in Table 1 and Figure 2. Elastic-plastic constitutive behavior with a distinct yield point was observed for all blends, accompanied by decreasing elongation with increasing GL content. However, even at 30% GL content, over 10% elongation is achieved with improved elastic modulus, which increased from 1.67 GPa in the case of neat mPP to 2.4-2.5 GPa for all GL blends. Previous studies show negligible improvement or even reduction in tensile strength without significant lignin modification or other compatibilizers, often citing issues such as lignin agglomeration or insufficient chemical bonding [12-14,19,21-24,26,34]. This work shows increased strength and modulus, close to or even exceeding predicted values using conventional analytical models for particulate composites (Figure S4, Supporting Information), while maintaining high elongation.

Micrographs show typical features of PP ductile failure at 10 wt% GL loading, meaning the plastic deformation mechanisms of PP are retained despite increased strength and stiffness (Figure 2b). A transition begins to occur at 20 wt% (Figure 2c), where the primarily ductile failure is interspersed with GL particles that represent stress concentrations; the inset in Figure 2c shows excellent bonding between mPP and GL, suggesting that interfacial debonding is not a significant issue. This behavior continues at 30 wt% loading, where the fibrils resulting from plastic deformation become shorter and sparser as the GL particles act as well-bonded discontinuities (Figure 2d). One possible explanation for the formation of GL agglomerates and subsequent decrease in failure strain is the formation of dense hydrogen bonding regions between GL particles, which is rich in carbonyl and hydroxyl groups [15,22,33]; see Section 3.1.3. for more discussion. Nevertheless, the formulation in this study clearly facilitates sufficient bonding for improved mechanical properties of mPP/GL blends.

3.1.3. Thermomechanical Properties

Dynamic mechanical analysis reveals the influence of lignin on the temperature- and frequency-dependent deformation behavior of polypropylene, giving insight into the structure-property relationship. Figure 3a shows the storage modulus (E'), loss modulus (E''), and loss factor ($\tan\delta$) for $f = 5$ Hz, which is close to the deformation rate employed in the static tensile testing. The values of E' for the materials in this study fall within 35% of the tensile modulus values (Table 1). The $\tan\delta$ (Figure 3a) and E'' (Figure 3b) peaks around 10 °C indicate the α-relaxation (T_α), also known as the glass transition (T_g); this relaxation process involves the cooperative motion of large chain segments and overlaps with the testing temperature ($T_r \approx 23$ °C). A slight shift to lower temperatures was observed upon addition of GL, but the primary change was

broadening of the T_α range as a function of strain rate, and strongly affects the temperature and frequency dependence of PP deformation approaching the melting point (secondary α-relaxation, or α'-relaxation), which is attributed to the covalent and hydrogen bonds formed between GL and mPP [41,42]. Additionally, the β-relaxation (-40~-80 °C) shifts to lower temperatures and exhibits significantly broader temperature ranges as GL content increases due to the presence of PEG ($T_g \approx$ -72 °C [43]). Arrhenius plots of these three relaxation peaks are shown in Figure 4c, from which the activation energies E_x were calculated (Figure 3d). These energy barriers are lower for lignin nanocomposite blends due to having more heterogeneous nano-structures [40].

The relationship between relaxation dynamics and static mechanical properties have been explored in-depth for metallic glasses [40], but only some trends have been observed for semi-crystalline polymers. Considering that inelastic deformation of the PP is primarily due to slippage between crystallites and strain-induced crystallization of amorphous chains [41,44], the activation energies of relaxation above T_g may provide insight into the effect of lignin on elongation behavior. Arrhenius plots of shift factors a_T (Figure S5, Supporting Information) revealed three distinct regions with different slopes (labeled *I*, *II*, and *III*), where the inflection points are temperatures at which dynamic mechanical behavior changes from glassy (*I*) to rubbery (*II*) to super-cooled melt (*III*) [42]. All three activation energies (E_I, E_{II}, and E_{III}) increased with GL content due to the constrained segmental motion. The strain at yield (ε_y) formed a linear trend with $E_{\alpha'}$ in Figure 3e such that higher GL content decreases ε_y, which may be explained by the reduced mechanical energy required to initiate inter-crystallite flow (i.e., plastic deformation) that occurs at higher temperatures ($\geq T_{\alpha'}$) and very low stresses [44]. Conversely, the strain at failure (ε_f) exhibited a sharp drop inversely proportional to E_{II},

since covalently bonded GL particles constrain the flow of amorphous PP and this increases the rupture probability at lower strains. The dynamic mechanical behavior of mPP/GL blends is illustrated in Figure 3f (see Supporting Information for more details).

3.2. Short Carbon Fiber Composites

3.2.1. Bulk Tensile Properties

In the case of mPP-CF (Table 1, Figure 4a), the tensile modulus increased with fiber content in the expected linear trend typical of discontinuous fiber composites [3,4]. Unlike unreinforced mPP-GL blends, ductile fracture was not observed in short fiber composites. Failure surfaces of the composites without GL reveal extensive interfacial debonding between PP and CF (Figure 4a, inset), indicating that MAH compatibilizer alone does not yield a high-strength interface.

Conversely, Figures 4b-d show significant improvement in both tensile strength and modulus when mPP-GL blends are used as a biomass-based matrix material. While tensile strength increased by 20% and 98% for mPP-GL20 and mPP-CF20, respectively, it increased by 138% for GL20-CF20—substantially higher than the expected 118% increase. The same trend is seen for all GL/CF composites (Table 1), which can be described as synergistic enhancement since the total increase is greater than the sum of the individual increases. The source of this behavior can be seen in the inset of Figure 4b, where exceptionally improved interfacial adhesion is manifested by the lack of bare fiber surface and cohesive failure in the matrix between fibers. This indicates that GL acts as a highly effective compatibilizer, allowing for light-weight composites with excellent mechanical properties simply by replacing synthetic plastic with GL biomass.

3.2.2. Nanomechanical Study

In order to further clarify the effect of GL on the mPP-GL-CF composite properties, a nanomechanical mapping technique was employed on mPP-CF20 and mPP-GL20-CF20. Figure 4e shows 5 × 5 μm^2 maps of the reduced elastic modulus near the fiber interface, which were calibrated using local nanoindentation measurements of fused quartz and polycarbonate standards. Although a slight increase in the modulus of the bulk mPP-GL blend can be deduced, and phase mapping implies a slightly different structure in the blend (Figure S6, Supporting Information), the main difference comes from the immediate vicinity of the interface.

Figure 4f shows the average linescan of the modulus across the fiber interface, where a region of approximately 125 nm-thickness exhibits a more gradual gradient when GL is present, resulting in two to three times higher modulus in the matrix near the fiber compared to neat mPP. Microscopy reveals that the GL particles in this study tend to fall between 100-1000 nm in diameter (Figures 3 and S7, Supporting Information), which is on the same scale as the thickness of the high-modulus region around the fibers. It is possible that GL is distributed more densely around the fibers compared to the bulk matrix as illustrated in Figure 4f, but no direct observations have been made to suggest this. As mentioned above, the majority of previous studies describe poor adhesion and agglomeration between lignin and polypropylene which leads to reduced mechanical properties, but the compounding process employed here produced well-dispersed GL blends with superior compatibility for carbon fiber composites due to the formation of a reinforced interphase layer near the fiber surface.

3.3. Industry Outlook

Comparison to previous reports on similar materials in terms of specific strength and specific stiffness is made in Figure 5. Several common thermoplastics such as PMMA,

PS, PLA, and PBAT show poor compatibility with lignin, resulting in low strength-to-weight ratios [11,14,16,23]. The low density and cost of polypropylene makes it an ideal material for automotive structures, where it may be reinforced with glass or carbon fibers to provide the required mechanical properties [3-5]. However, the interfacial strength has often been a major weakness, and lignin/polypropylene compatibility has consistently proved to be a difficult challenge for producing high-performance blends [21-24].

Our results show properties comparable to more highly-reinforced carbon fiber composites [5,47], while replacing 30% of the synthetic plastic with biomass GL. Although various chemical modifications can be made to both the GL and fibers to further improve the composite material performance, the cost efficiency from the user's perspective (i.e., the product manufacturer) and the environmental cost of convoluting the manufacturing process must be considered. If the mechanical and thermal properties of the blend are worse than neat polypropylene, industry will be reluctant to implement it; however, if the original properties are at least maintained or even improved, then replacing plastic with biomass is undeniably advantageous. Implementation of lignin blends would be revolutionary for the automotive industry, translating to a reduction in polypropylene use by 200-250 kilo-tons per year, mirrored by an increased utilization of biomass by the same amount. Although this manuscript focuses on automotive composites, the potential applications for lignin/polypropylene blends extend to numerous industries where lightweight, low-cost plastics are in demand, creating a greener society.

Conclusions

In this study, glycol lignin was compounded with maleic-anhydride-grafted polypropylene to produce GL/PP blends and their short carbon fiber composites. In addition to improved thermal stability, the mechanical properties were significantly improved, as confirmed by nanomechanical analysis and microscopy. A synergistic effect was observed, such that the combination of GL and carbon fiber resulted in greater improvement than the sum of their individual increases, which further indicated that GL forms a well-distributed network of bonds with MAH groups on the polypropylene, subsequently forming a stiff interphase around the fibers. The addition of 20% GL and 20% carbon fiber can achieve the same strength as 30% carbon fiber without GL. While the majority of previous studies show reduced mechanical properties at high lignin loading, this work has demonstrated that a simple manufacturing procedure with simple raw materials can yield exceptional results that have the potential to impact the sustainability of the automotive industry—and beyond.

Acknowledgement

This work was supported by MAFF (Ministry of Agriculture, Forestry and Fisheries), Japan commissioned project "Development of Glycol Lignin–Based High-Value-Added Materials", Grant Number J008722. The authors thank T. Kawano for assistance with sample preparation and C. Nagai and Y. Iida for assistance with nanoindentation.

References

1. W.J. Kissel, J.H. Han, J.A. Meyer, Polypropylene: Structure, Properties, Manufacturing Processes, and Applications; in: H. Karian (Ed.), Handbook of Polypropylene and Polypropylene Composites, Revised and Expanded, CRC Press, Boca Raton, 2003, pp. 10-27.

2. T. Thenepalli, A.Y. Jun, C. Han, C. Ramakrishna, J.W. Ahn, A strategy of precipitated calcium carbonate ($CaCO_3$) fillers for enhancing the mechanical properties of polypropylene polymers. Kor. J. Chem. Eng. 32 (2015),1009-1022, https://doi.org/10.1007/s11814-015-0057-3.

3. S.-Y. Fu, B. Lauke, E. Mäder, C.-Y. Yue, X. Hu, X. Tensile properties of short-glass-fiber- and short-carbon-fiber-reinforced polypropylene composites. Comp. Part A. 31 (2000) 1117-1125, https://doi.org/10.1016/S1359-835X(00)00068-3.

4. R. Várdai, T. Lummerstorfer, C. Pretschuh, M. Jerabek, M. Gahleitner, G. Faludi, J. Móczó, B. Pukánszky, Comparative study of fiber reinforced pp composites: effect of fiber type, coupling and failure mechanisms. Comp. Part A. 133 (2020) 105895, https://doi.org/10.1016/j.compositesa.2020.105895.

5. C. Unterweger, O. Brüggemann, C. Fürst, Effects of different fibers on the properties of short-fiber-reinforced polypropylene composites. Compos. Sci. Technol. 103 (2014) 49-55. https://doi.org/10.1016/j.compscitech.2014.08.014.

6. C.L. Wu, M.Q. Zhang, M.Z. Rong, K. Friedrich, Tensile performance improvement of low nanoparticles filled- polypropylene composites. Compos. Sci. Technol. 62 (2002) 1327-1340, https://doi.org/10.1016/S0266-3538(02)00079-9.

7. C.M. Chan, J. Wu, J.-X. Li, Y.-K. Cheung, Polypropylene/calcium carbonate nanocomposites. Polymer 43 (2002) 2981-2992, https://doi.org/10.1016/S0032-3861(02)00120-9.

8. K. Tamura, K. Naito, S. Nakayama, C. Nagai, T. Kitazawa, A. Yamagishi, Effect of maleic anhydride-grafted polypropylene on the morphological and mechanical

properties of clay/polypropylene nanocomposites. Clay Sci. 20 (2016) 31-37, https://doi.org/10.11362/jcssjclayscience.20.2_31.

9. C.M. Rochman, M.A. Browne, B.S. Halpern, B.T. Hentschel, E. Hoh, H.K. Karapanagioti, L.M. Rios-Mendoza, H. Takada, S. The, R.C. Thompson, Policy: Classify plastic waste as hazardous. Nature 494 (2013) 179-170, https://doi.org/10.1038/494169a.

10. A.K. Mohanty, S. Vivekanandhan, J.-M. Pin, M. Misra, Composites from renewable and sustainable resources: challenges and innovations. Science 362 (2018) 536-542, https://doi.org/10.1126/science.aat9072.

11. R. Chen, M.A. Abdelwahab, M. Misra, A.K. Mohanty, Biobased ternary blends of lignin, poly(lactic acid), and poly(butylene adipate-co-terephthalate): The effect of lignin heterogeneity on blend morphology and compatibility. J. Polym. Environ. 22 (2014) 439-448, https://doi.org/10.1007/s10924-014-0704-5.

12. M. Li, Y. Jia, X. Shen, T. Shen, Z. Tan, W. Zhuang, G. Zhao, C. Zhu, H. Ying, Investigation into lignin modified PBAT/thermoplastic starch composites: thermal, mechanical, rheological and water absorption properties. Ind. Crop. Prod. 171 (2021) 113916, https://doi.org/10.1016/j.indcrop.2021.113916.

13. M.A.S. Anwer, H.E. Naguib, A. Celzard, V. Fierro, Comparison of the thermal, dynamic mechanical and morphological properties of PLA-lignin & PLA-tannin particulate green composites. *Compos. Part B*. **2015**, *82*, 92-99. DOI: 10.1016/j.compositesb.2015.08.028.

14. Y.-L. Chung, J.V. Olsson, R.J. Li, C.W. Frank, R.N. Waymouth, S.L. Billington, E.S. Sattely, A renewable lignin-lactide copolymer and application in biobased

composites. ACS Sustain. Chem. Eng. 1 (2013) 1231-1238, https://doi.org/10.1021/sc4000835.

15. S.-J. Xiong, B. Pang, S.-J. Zhou, M.-K. Li, S. Yang, Y.-Y. Wang, Q. Shi, S.-F. Wang, T.-Q. Yuan, R.-C Sun, Economically competitive biodegradable PBAT/lignin composites: effect of lignin methylation and compatibilizer. ACS Sustain. Chem. Eng. 8 (2020) 5338-5346, https://doi.org/10.1021/acssuschemeng.0c00789.

16. M.A. Abdelwahab, S. Taylor, M. Misra, A.K. Mohanty, Thermo-mechanical characterization of bioblends from polylactide and poly(butylene adipate-co-terephthalate) and lignin. Macromol. Mater. Eng. 300 (2015) 299-311, https://doi.org/10.1002/mame.201400241.

17. Future Markets, Inc., The Global Market for Lignin 2021-2031 (Report 5331648). https://www.futuremarketsinc.com/the-global-market-for-lignin-2021-2031/, 2022 (accessed 5 May 2022).

18. D. Ye, J. Kong, S. Gu, Y. Zhou, C. Huang, W. Xu, X. Zhang, Selective aminolysis of acetylated lignin: toward simultaneously improving thermal-oxidative stability and maintaining mechanical properties of polypropylene. Int. J. Biol. Macromol. 108 (2018) 775-781, https://doi.org/10.1016/j.ijbiomac.2017.10.168.

19. D. Ye, S. Li, X. Lu, X. Zhang, O.J. Rojas, Antioxidant and thermal stabilization of polypropylene by addition of butylated lignin at low loadings. ACS Sustain. Chem. Eng. 4 (2016) 5248-5257, https://doi.org/10.1021/acssuschemeng.6b01241.

20. P. Buono, A. Duval, P. Verge, L. Averous, Y. Habibi, New insights on the chemical modification of lignin: Acetylation versus silylation. ACS Sustain. Chem. Eng. 4 (2016) 5212-5222, https://doi.org/10.1021/acssuschemeng.6b00903.

21. H. Sakai, K. Kuroda, S. Muroyama, T. Tsukegi, R. Kakuchi, J. Takada, A. Hata, R. Kojima, T. Ogoshi, M. Omichi, K. Ninomiya, K. Takahashi, Alkylated alkali lignin for compatibilizing agents of carbon fiber-reinforced plastics with polypropylene. Polym. J. 50 (2018) 281-284, https://doi.org/10.1038/s41428-017-0009-3.

22. F. Chen, H. Dai, X. Dong, J. Yang, M. Zhong, Physical properties of lignin-based polypropylene blends. Polym. Compos. 32 (2011) 1019-1025, https://doi.org/10.1002/pc.21087.

23. S.L. Hilberg, A.N. Elder, H. Chung, R.L. Ferebee, M.R. Bockstaller, N.R. Washburn, A universal route towards thermoplastic lignin composites with improved mechanical properties. Polymer 55 (2014) 995-1003, https://doi.org/10.1016/j.polymer.2013.12.070.

24. J.-S. Yeo, D.-W. Seong, S.-H. Hwang, Chemical surface modification of lignin particle and its application as filler in the polypropylene composites. J. Ind. Eng. Chem. 31 (2015) 80-85, https://doi.org/10.1016/j.jiec.2015.06.010.

25. S. Zhao, M.M. Abu-Omar, Synthesis of renewable thermoset polymers through successive lignin modification using lignin-derived phenols. ACS Sustain. Chem. Eng. 5 (2017) 5059-5066, https://doi.org/10.1021/acssuschemeng.7b00440.

26. O.A.T. Dias, M. Sain, I. Cesarino, A.L. Leão, Development of high bio-content polypropylene composites with different industrial lignins. Polym. Advan. Technol. 30 (2019) 70-78, https://doi.org/10.1002/pat.4444.

27. Y. Tang, M. Jean, S. Pourebrahimi, D. Rodrigue, Z. Ye, Influence of lignin structure change during extrusion on properties and recycling of lignin-polyethylene thermoplastic composites. Can. J. Chem. Eng. 99 (2021) 27-38, https://doi.org/10.1002/cjce.23960.

28. R. Gadioli, W.R. Waldman, M.A. De Paoli, Lignin as a green primary antioxidant for polypropylene. J. Appl. Polym. Sci. 133 (2016) 43558, https://doi.org/10.1002/app.43558.

29. A. Guilhen, R. Gadioli, F.C. Fernandes, W.R. Waldman, M.A. De Paoli, High-density green polyethylene biocomposite reinforced with cellulose fibers and using lignin as antioxidant. J. Appl. Polym. Sci. 134 (2017) 45219, https://doi.org/10.1002/app.45219.

30. N. Sallem-Idrissi, M. Sclavons, D.P. Debecker, J. Devaux, Miscible raw lignin/nylon 6 blends: thermal and mechanical performances. J. Appl. Polym. Sci. 133 (2016) 42963, https://doi.org/10.1002.app.42963.

31. M. Abdelwahab, M. Misra, A. Mohanty, Effect of maleated polypropylene emulsion on the mechanical and thermal properties of lignin-polypropylene blends. AIP Conf. Proc. 1664 (2015) 150006, https://doi.org/10.1063/1.4918502.

32. N. Ayrilmis, A. Kaymakci, Fast growing biomass as reinforcing filler in thermoplastic composites: paulownia elongata wood. Ind. Crop. Prod. 43 (2013) 457-464, https://doi.org/10.1016/j.indcrop.2012.07.050.

33. X. Xu, Z. He, S. Lu, D. Guo, J. Yu, Enhanced thermal and mechanical properties of lignin/polypropylene wood-plastic composite by using flexible segment-containing

reactive compatibilizer. Macromol. Res. 22 (2014) 1084-1089, https://doi.org/10.1007/s13233-014-2161-3.

34. C. Miao, W.Y. Hamad, Controlling lignin particle size for polymer blend applications. J. Appl. Polym. Sci. 134 (2017) 44669, https://doi.org/10.1002/app.44669.

35. T.T. Nge, T. Yamada, Y. Tobimatsu, M. Yamamura, R. Ishii, O. Tanaike, T. Ebina, Fractionation and characterization of glycol lignins by stepwise-pH precipitation of Japanese cedar/poly(ethylene glycol) solvolysis liquor. ACS Sustain. Chem. Eng. 9 (2021) 756-764, https://doi.org/10.1021/acssuschemeng.0c06892.

36. T.T. Nge, Y. Tobimatsu, S. Takahashi, E. Takata, M. Yamamura, Y. Miyagawa, T. Ikeda, T. Umezawa, T. Yamada, Isolation and characterization of polyethylene glycol (PEG)-modified glycol lignin via PEG solvolysis of softwood biomass in a large-scale batch reactor. ACS Sustain. Chem. Eng. 6 (2018) 7841-7848, https://doi.org/10.1021/acssuschemeng.8b00965.

37. K. Ono, O. Tanaike, R. Ishii, T. Nakamura, K. Shikinaka, T. Ebina, T.T. Nge, T. Yamada, Solvent-free fabrication of an elastomeric epoxy resin using glycol lignin from Japanese cedar. ACS Omega 4 (2019) 17251-17256, https://doi.org/10.1021/acsomega.9b01884.

38. O. Tanaike, K. Ono, R. Ishii, T. Ebina, S. Takahashi, T.T. Nge, T. Yamada, Unique gelation of polyethylene glycol-modified lignin in hot ethanol and its application to the synthesis of epoxy resin with a large lignin content. Ind. Eng. Chem. Res. 60 (2021) 17045-17054, https://doi.org/10.1021/acs.eicr.1c03269.

39. Kawamura, T.; Miyamoto, M. Composition of a Polyolefin Resin and its Application as Gas Barrier Material *(in Japanese)*. JP 2016-141793 A.

40. W.H. Wang, Dynamic relaxations and relaxation-property relationships in metallic glasses, Prog. Mater. Sci. 106 (2019) 100561, https://doi.org/10.1016/j.pmatsci.2019.03.006.

41. K. Li, B. Xiong, Y. Cao, Influence of temperature on the microstructure and mechanical properties of stretched polypropylene, J. Appl. Polym. Sci. 132 (2015) 42622, https://doi.org/10.1002/app.42622.

42. D.P. Harper, M.P.G. Laborie, M.P. Walcott, The impact of polypropylene-*graft*-maleic anhydride on the crystallization and dynamic mechanical properties of isotactic polypropylene, J. Appl. Polym. Sci. 111 (2009) 753-758, https://doi.org/10.1002/app.29100.

43. H.J. Oh, B.D. Freeman, J.E. McGrath, C.H. Lee, D.R. Paul, Thermal analysis of disulfonated poly(arylene ether sulfone) plasticized with poly(ethylene glycol) for membrane formation, Polymer 55 (2014) 235-247, https://doi.org/10.1016/j.polymer.2013.11.041.

44. C. Stern, A. Frick, G. Weickert, Relationship between the structure and mechanical properties of polypropylene: Effects of the molecular weight and shear-induced structure, J. Appl. Polym. Sci. 103 (2007) 519-533, https://10.1002/app.24156.

45. W. Woigk, Y. Nagel, S. Gantenbein, F.B. Coulter, K. Masania, A.R. Studart, Flax-based natural composites hierarchically reinforced by cast or printed carbon fibres, Compos. Sci. Technol. 226 (2022) 109527, https://doi.org/10.1016/j.compscitechn.2022.109527.

Figure 1. (a) Outline of manufacturing process for glycol lignin/MAH-*g*-PP blends and their short carbon fiber composites via melt extrusion. (b) Schematic depiction of proposed structure and (c) FTIR spectra of GL, mPP, and mPP/GL blends.

Figure 2. (a) Tensile properties of mPP/GL blends, (b) fracture surface of neat mPP, and fracture surfaces of blends with (c) 10 wt%, (d) 20 wt%, and (e) 30 wt% GL content. *(Scale bars: 20 μm, insets: 1 μm.)*

Figure 3. (a) Representative E', E'' and $\tan\delta$ curves for f = 5 Hz. (b) E'' curves showing shifts in β-relaxation and broadening of α'-relaxation. (c) Arrhenius plots of relaxation and schematic of lignin effect on β- and α-transitions. (d) Decrease in relaxation activation energies with increasing GL content. (e) Trend between yield strain and failure strain, and activation energies. (f) Illustration of GL effect on PP chain dynamics; original and current configurations are denoted by dashed and solid lines, respectively.

Figure 4. Tensile behavior of short fiber composites (a) without and (b) with GL (*scale bars: 20 μm*), and a summary of (c) modulus and (d) strength for all compositions. (e) Reduced modulus map for mPP-CF20 and mPP-GL20-CF20, and (f) line scan of reduced modulus across the fiber interface (inset shows a magnified view near the interface).

Figure 5. Specific stiffness vs specific strength comparison of lignin-thermoplastic composites. (Data taken from references [11,14,16,22,23,27,34].)

Table 1. Tensile properties of mPP-GL blends and their carbon fiber composites.

Material	Density (g/cm^3)	Tensile Modulus (GPa)	Tensile Strength (MPa)[a]	Failure Strain (%)
mPP	0.91	1.81(±0.08)	34.1(±0.78)	989(±111)
mPP-GL10	0.92	2.49(±0.04) *(37.6%)*[b]	39.7(±2.8) *(16.4%)*	927(±86)
mPP-GL20	0.95	2.45(±0.06) *(35.4%)*	41.2(±0.10) *(20.8%)*	267(±35)
mPP-GL30	0.98	2.52(±0.43) *(39.2%)*	42.2(±1.5) *(23.8%)*	21.1(±4.3)
mPP-CF10	0.94	6.61(±0.87) *(265%)*	52.8(±2.6) *(54.8%)*	3.53(±0.64)
mPP-CF20	0.99	9.46(±0.79) *(423%)*	67.8(±1.3) *(98.8%)*	3.05(±0.48)
mPP-CF30	1.04	11.8(±0.92) *(554%)*	82.6(±2.6) *(142%)*	2.94(±0.83)
mPP-GL10-CF10	0.98	7.80(±0.93) *(331%)*	60.9(±2.1) *(78.6%)*	2.89(±0.34)
mPP-GL10-CF20	1.02	10.9(±1.1) *(501%)*	77.1(±1.5) *(126%)*	2.54(±0.46)
mPP-GL20-CF10	1.01	8.35(±0.97) *(361%)*	65.4(±1.1) *(91.8%)*	2.80(±0.19)
mPP-GL20-CF20	1.06	9.66(±1.2) *(432%)*	81.0(±1.8) *(138%)*	2.45(±0.22)
mPP-GL30-CF10	1.05	9.23(±1.0) *(410%)*	69.9(±2.2) *(105%)*	2.18(±0.16)
mPP-GL30-CF20	1.10	12.6(±1.2) *(593%)*	83.3(±1.9) *(144%)*	1.68(±0.11)

[a] *The yield stress is taken as the ultimate strength, but occasionally these two values differ.*
[b] *(%) represents the relative increase with respect to neat mPP.*

Figure

Click here to access/download;Figure;Figures.docx

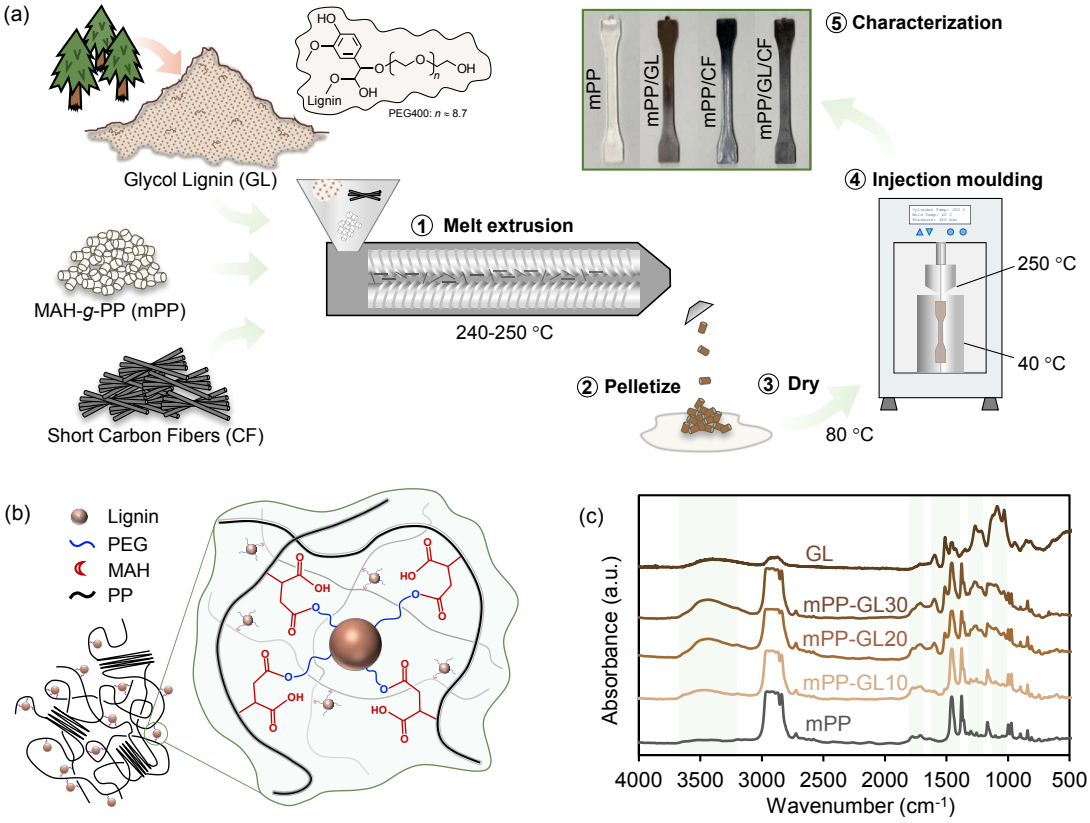

FIG 1

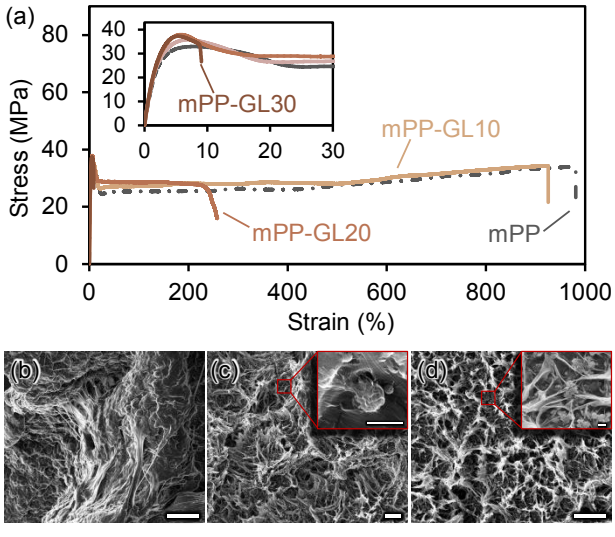

FIG 2

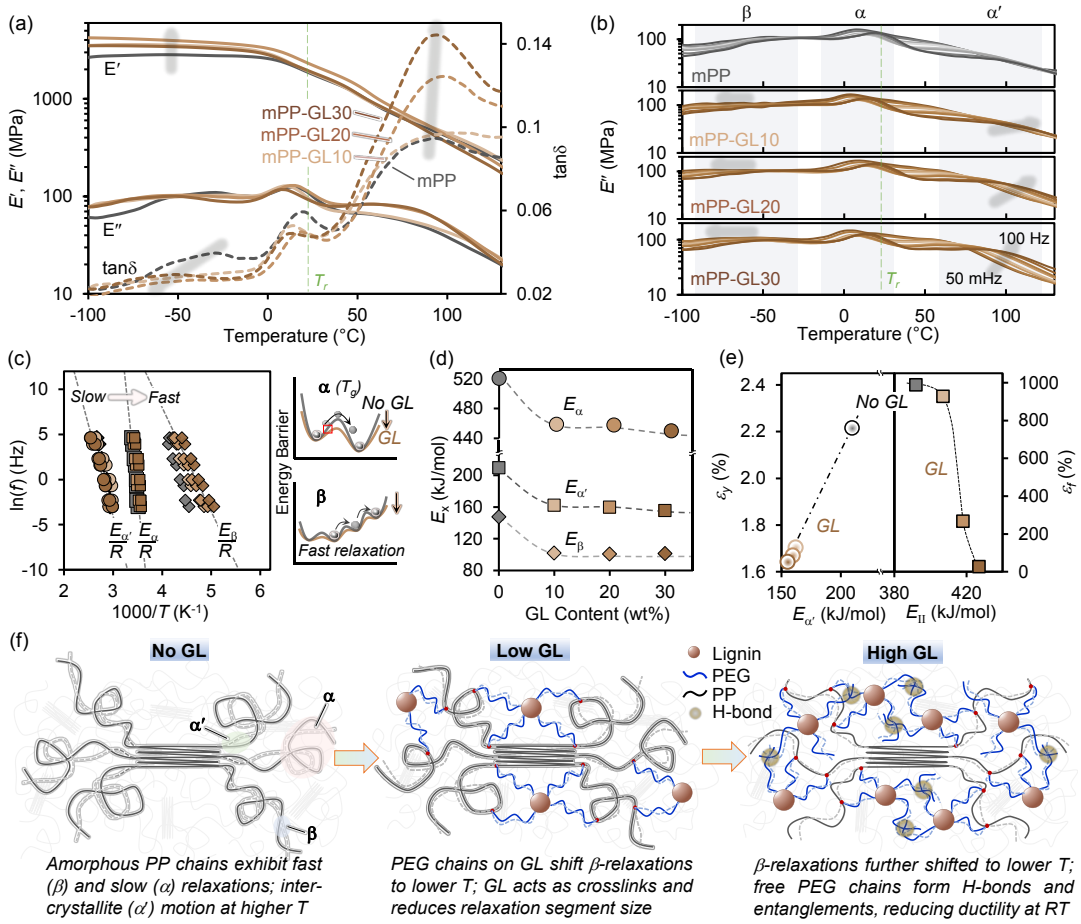
(a)
E′
E″
tanδ
mPP-GL30
mPP-GL20
mPP-GL10
mPP
E′, E″ (MPa)
tanδ
Temperature (°C)
(b)
β
α
α′
mPP
mPP-GL10
mPP-GL20
mPP-GL30
100 Hz
50 mHz
E″ (MPa)
Temperature (°C)
(c)
Slow
Fast
ln(f) (Hz)
1000/T (K⁻¹)
α (Tg)
No GL
GL
β
Fast relaxation
Energy Barrier
(d)
Eα
Eα′
Eβ
Ex (kJ/mol)
GL Content (wt%)
(e)
No GL
GL
GL
εγ (%)
εf (%)
Eα′ (kJ/mol)
EII (kJ/mol)
(f)
No GL
Low GL
High GL
Lignin
PEG
PP
H-bond
α
α′
β
Amorphous PP chains exhibit fast (β) and slow (α) relaxations; inter-crystallite (α′) motion at higher T
PEG chains on GL shift β-relaxations to lower T; GL acts as crosslinks and reduces relaxation segment size
β-relaxations further shifted to lower T; free PEG chains form H-bonds and entanglements, reducing ductility at RT

FIG 3

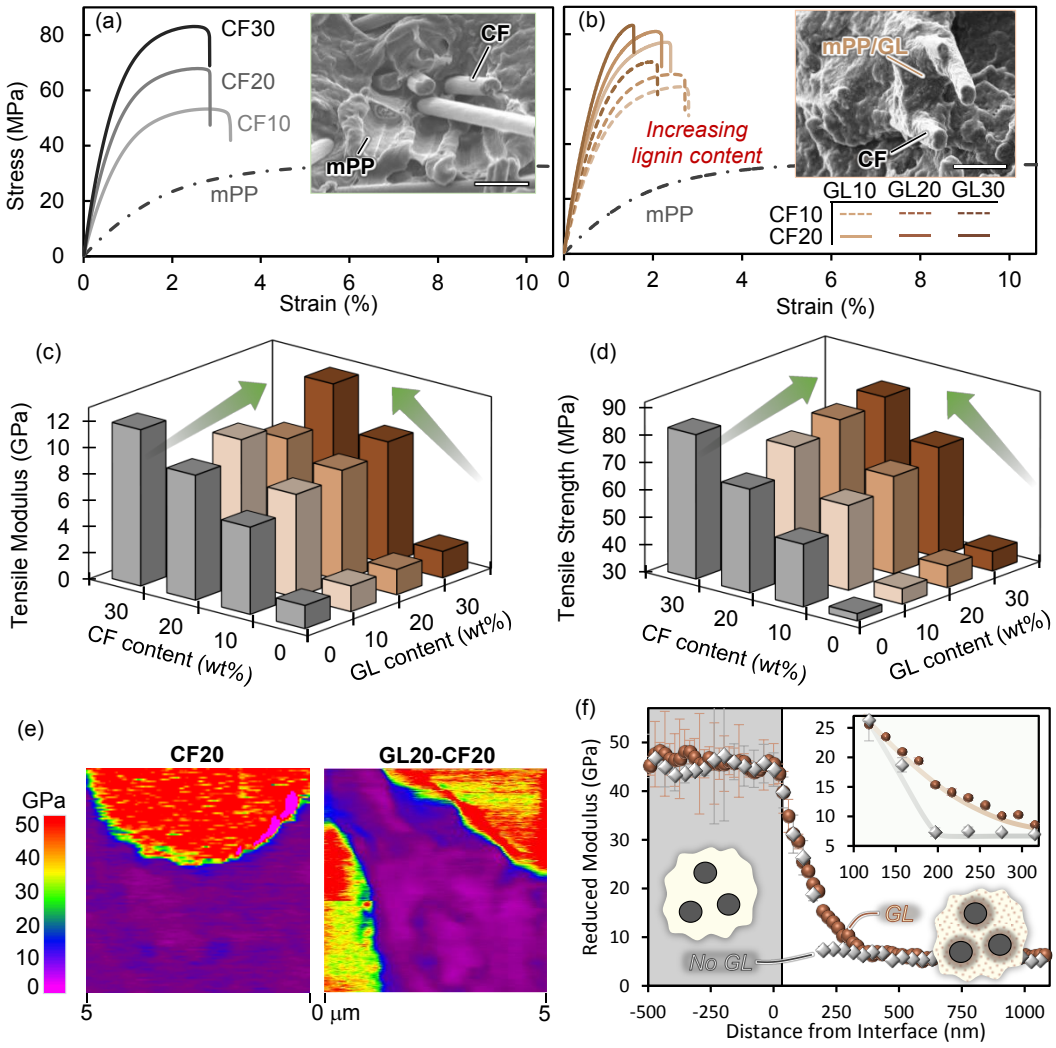
(a)
CF30
CF20
CF10
mPP
CF
mPP
Stress (MPa)
Strain (%)
(b)
Increasing lignin content
mPP
mPP/GL
CF
GL10 GL20 GL30
CF10
CF20
Strain (%)
(c)
Tensile Modulus (GPa)
CF content (wt%)
GL content (wt%)
(d)
Tensile Strength (MPa)
CF content (wt%)
GL content (wt%)
(e)
CF20
GL20-CF20
GPa
0 μm
(f)
Reduced Modulus (GPa)
No GL
GL
Distance from Interface (nm)

FIG 4

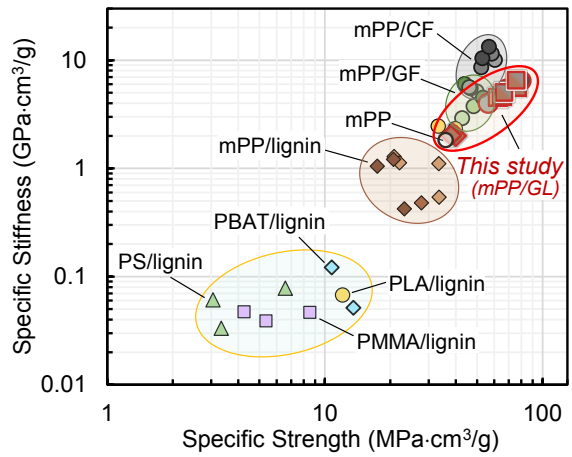
mPP/CF
mPP/GF
mPP
mPP/lignin
This study
(mPP/GL)
PBAT/lignin
PS/lignin
PLA/lignin
PMMA/lignin
Specific Stiffness (GPa·cm³/g)
Specific Strength (MPa·cm³/g)

FIG 5